Article:
Liu, Z, Li, Z, Zhai, H et al. (2021) A highly sensitive stretchable strain sensor based on multi-functionalized fabric for respiration monitoring and identification. Chemical Engineering Journal, 426. 130869. ISSN: 1385-8947

https://doi.org/10.1016/j.cej.2021.130869

A highly sensitive stretchable strain sensor based on multi-functionalized fabric for respiration monitoring and identification

Zekun Liu[a,b], Zhenhong Li[c], Heng Zhai[a], Lu Jin[a], Kaili Chen[d], Yangpeiqi Yi[a], Yuan Gao[b], Lulu Xu[a], Yan Zheng[a], Sirui Yao[a], Zhangchi Liu[a], Gang Li[e], Qingwen Song[f], Pengfei Yue[f], Shengquan Xie[c], Yi Li[a*], and Zijian Zheng[b*]

[a] Department of Materials, University of Manchester, Oxford Road, Manchester, M13 9PL, UK.

[b] Laboratory for Advanced Interfacial Materials and Devices, Research Center for Smart Wearable Technology, Institute of Textiles and Clothing, The Hong Kong Polytechnic University, Hong Kong S. A. R., China.

[c] School of Electrical and Electronic Engineering, University of Leeds, Leeds LS2 9JT, UK.

[d] Department of Materials, Imperial College London, SW7 2AZ, UK.

[e] National Engineering Laboratory for Modern Silk, Soochow University, Suzhou, 215123, China.

[f] School of Textile Science and Engineering, Xi'an Polytechnic University, Xi'an 710048, China

Corresponding Authors E-mail: henry.yili@manchester.ac.uk, tczzheng@polyu.edu.hk

Abstract

Wearable strain sensors have generated considerable recent research interest due to their huge potential in the real-time detection of human body deformation. State-of-the-art strain sensors are normally fabricated through conductive networks with a single sensing element, which always faces the challenge of either limited stretchability or inferior quality in sensitivity. In this work, we report a highly sensitive strain sensor based on a multi-functionalized fabric through carbonization and polymer-assisted copper deposition. The sensor shows high sensitivity (Gauge factor~3557.6 in the strain range from 0 to 48%), and outstanding

stretchability up to the strain of 300%, which is capable of detecting different types of deformation of the human body. By integrating the high-performance sensor with a deep learning network, we demonstrate a high-accuracy respiration monitoring and emergency alarm system, showing the enormous application potential of the sensor in personal and public healthcare.

Keywords: strain sensor, fiber functionalization, wearable electronics, copper deposition, sensitivity enhancement

1. Introduction

Human activity and health monitoring with skin-mountable and stretchable strain sensors fulfilled in a continuous and timely manner are attracting considerable research interest on account of their great possible benefits.[1-4] Much research in recent years has focused on resistance-based strain sensors due to the easy and low-cost fabrication process as well as the high sensitivity.[5, 6] Numerous experiments attempted to fabricate the strain sensors via constructing conductive network configuration with the encapsulation of elastomers. Such conductive network configuration can be implemented through electrostatic spinning, wet spinning, and surface chemical etching, which is often time-consuming and technically difficult.[7-10]

Recently, it was found that β-sheet-rich silk protein and polymers would be transformed into pseudographitic structures through simple heat treatment, which aroused much attention for developing wearable sensors.[11-18] Nevertheless, the carbonized polymer-based strain sensors detecting applied strain as a function of contact resistance changes face the challenge of either limited stretchability or inferior quality in sensitivity. For example, a strain sensor made with carbonized cotton fabric showed a stable strain sensing ability up to the strain of 80%.[12] Another carbonized silk fabric sensor indicated a low gauge factor (GF) of 9.6 in the sensing range within 250%.[11] More importantly, human motion monitoring with strain sensors lacks the function of signal recognition, which is far from optimal in the practical application scenario. It is of vital importance to develop a strain sensor with the performance of high sensitivity and stretchability to reliably convert surface movements into electrical

signals, and the ability of signal identification to precisely alarm emergency.

Herein, we report a highly sensitive wearable strain sensor with good stretchability through polymer-assisted metal deposition (PAMD) on linen fabric with high-temperature processing. The high-performance strain sensor is readily fabricated by depositing highly conductive copper particles on a carbonized fabric (CF), then encapsulated with Ecoflex. The intermingled copper distributed on the fiber surface endows the sensor with outstanding performance. For instance, the GF of the sensor is ~3557.6 and ~47.8 in the strain range from 0 to 48% and from 48% to 150%, respectively. It also enables the sensor to achieve a large stretchability up to the strain of 300%. By taking advantage of the high sensitivity and stretchability, the copper-deposited carbonized fabric (CDCF) sensor with multi-sensing elements (i.e. copper particles and conductive fiber) enables to detect many human motions in real time. We also demonstrate a respiratory monitoring and warning system constructed with the sensor and a deep learning network to monitor and identify normal breath, tachypnea as well as tachypnea with cough, revealing enormous potential in the healthcare of people with respiratory diseases such as COVID-19 infected patients.

2. Experimental Section

2.1. Fabric functionalization and sensor fabrication

The pristine linen woven fabrics (supplied by the textile lab of the University of Manchester) were carbonized in a tube furnace at a heat-up speed of 3°C/min with the protection of nitrogen throughout. When reaching the target temperature, the fabric was naturally cooling

down to room temperature before taking out. The CFs were then immersed in concentrated sulfuric acid at 80°C for 1 h to increase functional groups for following-step polymer growth. After that, the retreated CFs were treated in a 4 % (v/v) [3-(methacryloyloxy) propyl] trimethoxysilane solution (solvent: 95 % ethyl alcohol, 1% acetic acid, and 4 % deionized water) in room temperature for 2 h. After that, the silanized CFs were then dipped into 50 mL mixed solution at 80°C for 1 h, the solution contains ([2-(methacryloyloxy) ethyl] trimethyl ammonium chloride (METAC) (10 mL), deionized water (40 mL), and potassium persulfate (100 mg). Then, the CFs were immersed in the aqueous solution of $(NH_4)_2PdCl_4$ (5×10^{-3} M L^{-1}) in a dark environment for the growth of the activator for following copper deposition. Finally, the $[PdCl_4]^{2-}$ loaded CFs were immersed into a mixture of isometric A and B for 40 min to achieve copper deposition. A is NaOH (12 g L^{-1}), $CuSO_4\cdot5H_2O$ (13 g L^{-1}), and $KNaC_4H_4O_6\cdot4H_2O$ (29 g L^{-1}) in deionized water, B is formaldehyde aqueous solution (9.5 mL L^{-1}). To explore the concentration of the A and B solutions in determining the conductivity of the CDCF, the concentration of both solution A and B was decreased by half and twice as the abovementioned parameters respectively. The detailed mechanism discussion of the PAMD can be found in our previous study.[3, 19, 20] To fabricate the CF and CDCF sensors, both CF and CDCF were cut into the size of 2.2×1 cm^2 with silver paste and conductive tape at both ends. After the encapsulation with Ecoflex, the sensors were cured at room temperature for 24 h.

2.2. Characterization

The surface morphology of pristine fabric, CF, and CDCF was observed by an optical microscope (Keyence VHX-5000) and a scanning electron microscope (ZEISS Ultra-55). The

atomic percentage of the surface elements of all the samples was detected by the scanning electron microscope (ZEISS Ultra-55) equipped with energy-dispersive X-ray spectroscopy (EDS), and the voltage during the measurement is 10 V. A Raman spectroscopy (WITec, Apyron) with a 532 nm laser wavelength and a transmission electron microscope (Tecnai T20) were used to measure the structure of the CF. The sheet resistance of the CFs and CDCFs was measured through Keithley 2450 equipped with four-point probes and programmable software purchased from Beijing Hanlei Technology co. LTD. Targeted strain applied on the sensors was achieved by a universal mechanical instrument (Instron 3344), and all electrical signals generated from sensors were collected by a multimeter (Keithley 2000).

3. Results and discussion

3.1. Fabric functionalization and sensor fabrication

Fig. 1a shows the procedure of functionalizing a highly conductive composite from a piece of commercial linen fabric. The fabric is firstly treated in the inert gas environment (700°C) to induce the structure transformation, then experience the modification by functional polymers, that is, silane-type initiator and METAC, following with ion pairing with palladium moieties as the activator. After that, dense copper nanoparticles onto the carbonized fiber are fulfilled from the polymer layers (Details in Experimental Section). Even though experiencing carbonization and copper deposition, the fabric still maintains good flexibility, both of which can be folded into a collar shape (Fig. 1b). To fabricate the CDCF sensor, the CDCF in the size of 2.2×1 cm^2 with silver paste and conductive tape at both ends is encapsulated with Ecoflex (Fig. 1c). Fig. S1 exhibits that the overall thickness of the sensor is about 850 μm,

and all the multi-functionalized fibers are well encapsulated.

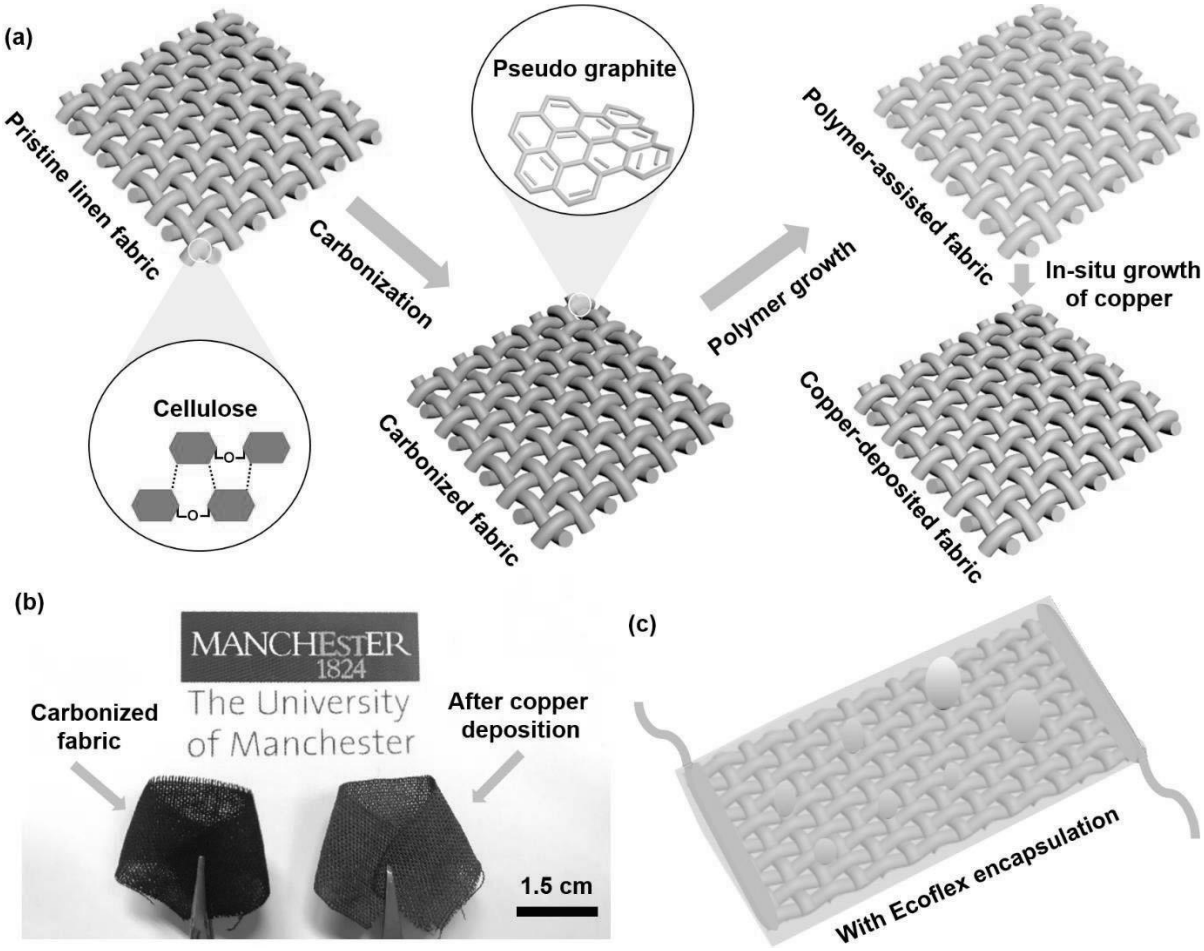

Fig. 1. The schematic diagrams of fabrication of the CDCF sensor. a) The procedures of producing multi-conductive fabric through carbonization and PAMD. b) The photographs of the CF and CDCF, showing their robustness and flexibility by bending them into collar shape. c) The fabrication of the CDCF sensor by encapsulating the CDCF with liquid Ecoflex.

With the carbonization and PAMD, the surface morphology and microstructure of the fabric are significantly changed. Fig. S2a, b illustrate that the pristine fabric (11×2.2 cm^2) experiences a surface shrinkage after carbonization (7×1.5 cm^2), which can be attributed to the release of CO_2, CO as well as H_2O during heat treatment. After PAMD, there is a layer of visible copper-like elements on the surface of the fabric (Fig. S2c). Higher-magnification

morphology in Fig. 2a, b suggests that the surface of both pristine and carbonized linen fibers is smooth, and there is a volume shrinkage after experiencing thermal treatment, while many dense particles are attached to the surface of fibers after PAMD (Fig. 2c). The process of the fabric functionalization significantly changes the surface elements, of which atomic percentage of C, O, and N is 42.7%, 51.9%, and 0.9% respectively for the pristine fabric, while that of them becomes 93.5%, 6.2%, and 0.2% with thermal treatment (Fig. 2d). After copper deposition, the chemical elements change into C, O, and Cu with the atomic percentage of 10.8%, 2.6%, and 86.5% respectively. There is a layer of dense copper particles at the surface of the carbonized fiber after PAMD. The surface elements mainly include Cu, C, and O, and the N is too low to be detected. The elements conversion is also characterized by observing their distribution, it shows that the corresponding elements are even-distributed throughout without agglomeration (Fig. S3, Fig. 2e).

The heating process in the inert gas atmosphere not only changes the surface morphology and chemical elements but also results in the structural transformation from cellulose to carbonaceous forms, which is validated by Raman spectroscopy as well as transmission electron microscopy (TEM). A typical TEM image of the CF shown in Fig. 2f exhibits many tiny distorted lattice stripes with an interlayer distance of ~0.35 nm, revealing the formation of pseudo-graphitic structure induced by heat treatment.[11, 18] We carbonize the pristine fabrics in the temperature of 700°C, 900°C, and 1100°C respectively, and then the CFs are modified with PAMD for the fabrication of CDCF sensors. The sheet resistance of the carbonized fabrics with the treatment of 700°C, 900°C, and 1100°C is 5.6×10^{3} Ω sq^{-1}, 21.36

Ω sq^{-1}, and 12.69 Ω sq^{-1} respectively, indicating that high-temperature treatment not only promotes a high degree of structural order in the integrity of the graphite but also increase their conductivity. The sheet resistance of the CDCF (700°C) for the fabrication of the sensor is 1.3×10^{-2} Ω sq^{-1} after PAMD. The conductivity is very flexible to control by changing the concentration of the reaction solution (Details in Experimental Section). With decreasing the concentration, the sheet resistance of the CDCF and surface atomic percentage of copper is 8.9×10^{-2} Ω sq^{-1} and 69.54% respectively (Figure S4a). By contrast, they become 1.2×10^{-2} Ω sq^{-1} and 89.63% respectively by increasing the concentration of the reaction solution (Figure S4b). The Raman spectra in Fig. 2g and Fig. S5a reveal that there are two distinct characteristic peaks of graphite for all the heat-treated fabrics, which represent typical G-band and D-band located at ~1584 cm^{-1} and ~1330 cm^{-1} respectively, additionally manifesting the formation of carbonaceous structure. The change of the G-band and D-band with the increase of temperature shows that higher temperature promotes a higher degree of structural order in the integrity of the graphite. By fitting the curves of the Raman spectra (Fig. S5b-d), the intensity ratios of D-band and G-band (I_D/I_G) increase as a function of temperature increase (Fig. S5e), of which findings are consistent with reported work.[13] The sheet resistance of the carbonized fabrics with the treatment of 700°C, 900°C, and 1100°C is 5.6×10^{3} Ω sq^{-1}, 21.36 Ω sq^{-1}, and 12.69 Ω sq^{-1} respectively, indicating that high-temperature treatment not only promotes a high degree of structural order in the integrity of the graphite but also increase their conductivity. The mechanical property of the fabric significantly decreases after the carbonization. Fig. S6a exhibits that the pristine fabric possesses a breaking strength of more than 10 MPa, while it becomes ~153 kPa and ~212 kPa for the CF

(700°C) and the CDCF respectively (Fig. 2h). The slight increase in breaking strength after the PAMD can be ascribed to the uniform polymer interfacial layer (i.e., METAC) that bonds the metal to the CF surface. In addition, Fig. S6b shows that the breaking strain and breaking stress of the CF (900℃) are ~140 kPa and ~13% respectively, while those of the CF (1100℃) are ~100 kPa and ~10% respectively. By comparing the mechanical performance of the CF treated with 700℃, it indicates that higher temperature treatment would decrease the both breaking strain and breaking stress of the CF.

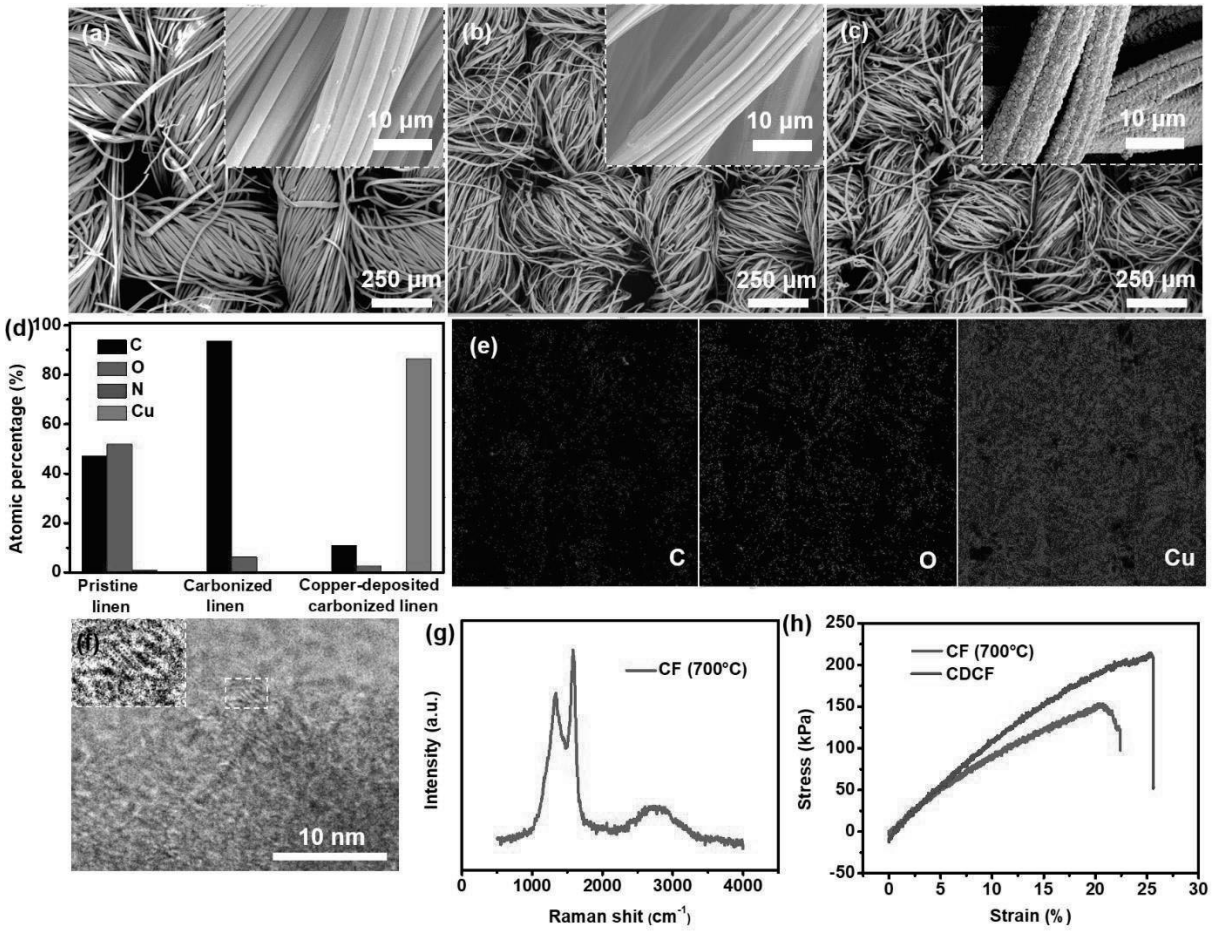

Fig. 2. Characterization of pristine and functionalized linen fabrics. a) Surface morphology of pristine linen fabric. b) Surface morphology of the CF. c) Surface morphology of the CDCF. d) The surface elements of pristine linen fabric, and the CF as well as the CDCF. e) The surface element distribution of the CDCF. f) TEM image of the CF, showing its carbonaceous

structure. g) Raman spectra of the CF after the treatment of 700°C in an inert gas atmosphere. h) The strain-stress curves of the CF and CDCF.

3.2. Calibration and sensing mechanism of the CDCF sensor

Before the calibration of all sensors, a tensile strain with a speed of 5 mm/min served as rupturetrainning was applied until the resistance of them is infinite (CF sensor) or stable (CDCF sensor). Fig. S7 presents the photographs of the CDCF sensor at the tensile strain of 0%, ~40%, and ~150%, showing the formation of strain-dependent deformation. Calibration results in Fig. 3a exhibit that the CF sensor acquires a low sensitivity with tolerable strain up to 96%, of which GF is only ~23.0 throughout the sensing range (See sensitivity details of all sensors in Table S1). The sensitivity of strain sensors is indicated by the GF, which is defined as $GF=(_{\Delta}R/R_0)/\varepsilon$, where the ε is the strain of the strain sensor. The resistance of the electrical network in the sensor would be infinite with further stretching. By contrast, the sensor made with CDCF (700°C) shows remarkable sensitivity (GF~3557.6 in the strain range from 0 to 48%, GF~47.8 in the strain range from 48% to 150%), and outstanding stretchability up to 300% (Fig. S8). The electrical response of the sensor in the tensile strain ranging from ~150 % to ~300 % shows very little change, it cannot detect strain changes in this range. However, this property is still very important for wearable sensors, as it would avoid the sensor being damaged in real application when deformation over the strain of ~150%. Fig. 3b displays that there is the formation of small cracks on the CDCF network after the rupturetrainning, and they gradually extend with increasing stretching, thus leading to an increase in resistance. The multi-layer sensing elements (i.e. copper and carbonized fiber) with the significant

difference in conductivity are of vital importance to the high sensitivity and stretchability. Both of the CDCF sensors with the carbonization temperature of 900°C and 1100°C present a lower sensitivity than the sensor treated with 700°C (Fig. S9), as higher temperature promotes higher conductivity of CF, thus resulting in the smaller relative change in resistance at the same-extent elongation.

The schematic diagram of the CDCF sensor in Fig. 3c illustrates that elongation-induced fractured fiber and copper particles experience separation, and some suspended fibers perpendicular to the tensile direction maintain the conductive pathway. Notably, unlike the CF sensor with limited stretchability, the CDCF sensor is capable of suffering a larger degree of tensile strain up to 300%, which profits from the retention of copper particles (attached to the suspended fibers) in the crack gap. The sensor shows consistent electrical signals at a high degree of strain (>150%) because the further elongation fails to accelerate the separation of fractured fiber, which is consistent with the observation of the reported strain sensor.[5] To understand the sensitivity enhancement by introducing copper, the electrical models of the CDCF sensor and CF sensor are illustrated in Fig. 3d and Fig. S10 respectively. According to the circuits, the equivalent resistance of the CDCF and CF sensors can be calculated with Equation (1) and Equation (2) respectively.[11, 21, 22]

$$R= (2R_1R_2+ R_1R_3+R_2R_3)/(R_1+R_2+2R_3) \quad (1)$$

$$R= (R_xR_c+ 2R_xR_y+2R_cR_y)/(R_x+R_c) \quad (2)$$

Where R_1, R_2, and R_3 represent the resistance of copper in the island, carbonized fiber, and copper in gap regions respectively. R_x, R_y, and R_c refer to the CF resistance of suspended

bridge fiber, island fiber, and fractured fiber respectively. Elongation deformation would both increase the R_2 and R_3 for the CDCF sensor, while it only enhances the R_c for the CF sensor. More importantly, the same degree of stretching induces a larger relative change in resistance for the CDCF sensor due to the high conductivity of copper, thus the CDCF sensor acquires superior sensitivity.

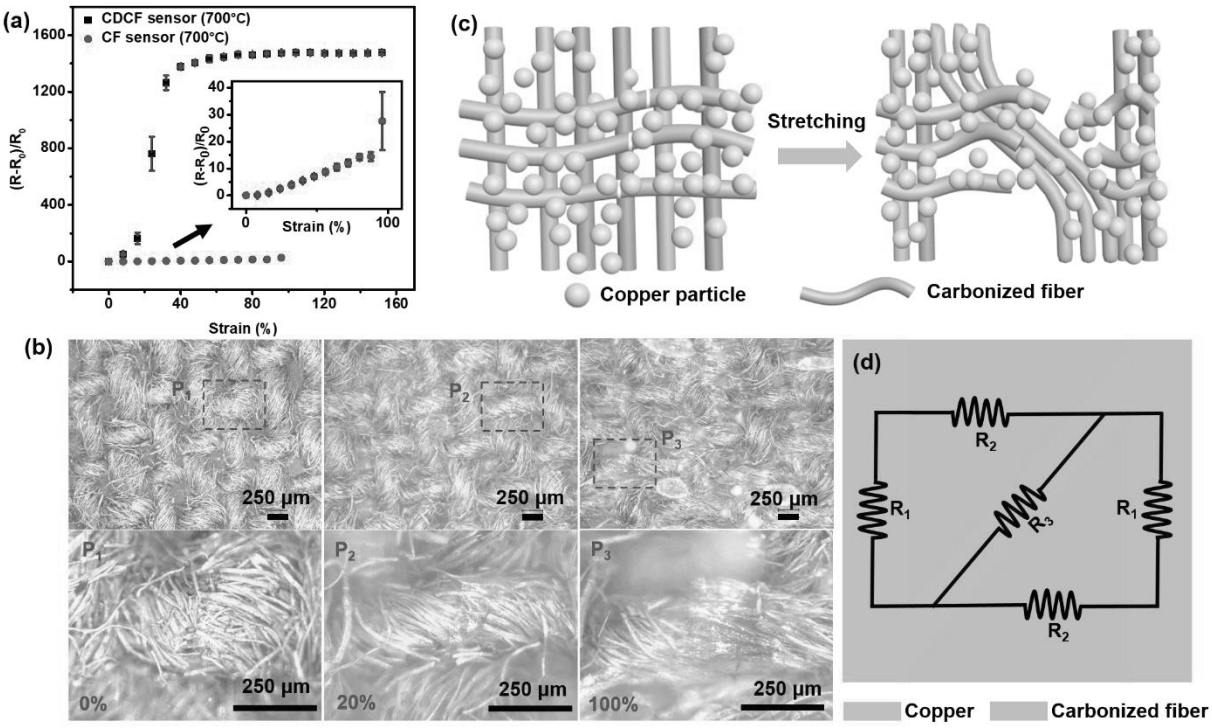

Fig. 3. Electrical responses of the CF sensor, CDCF sensor, and corresponding mechanism. a) Calibration results of the CF and CDCF sensors, showing the sensitivity enhancement after copper deposition. b) The microsphere image of the CDCF sensor under the tensile strain of 0%, 20%, and 100%. c) Schematic illustration of the CDCF sensor in original and stretched states, and d) electrical model of the sensor, showing its sensing mechanism.

3.3. Electromechanical performance

Because of the higher sensitivity and stretchability of the CDCF (700°C) sensor, further

performance investigation and demonstration would mainly focus on it without explanation. To evaluate the sensing reliability in a dynamic process, we tested the electrical response of the sensor under cyclic loading-unloading in various frequencies and strains. Fig. 4a shows that the signal generated from the sensor is reproducible at a certain strain, and consistent with calibration results. We also applied a periodic stretching–releasing strain of 10% with the frequency of 0.1 Hz, 0.5 Hz, and 1 Hz respectively. The response shown in Fig. 4b is also stable with marginal fluctuation, indicating the sensor enables to reliably detect applied strain throughout the sensing range. By applying the tensile strain of 12.5% and 60% in 2.5 s, and maintaining the elongation, the signals are capable of reflecting the corresponding deformation, showing the real-time perception ability of the sensor (Fig. 4c).

To precisely evaluate the response speed, a quasi-transient step strain of 0.5% with the speed of 16 mm/s was applied to the sensor. The fractional change in resistance shows that the response time reaches ~225 ms (Fig. 4d), which can meet the general sensing requirements of many daily motions. Remarkably, Fig. S11 shows that when applying a strain of 0.1% onto the CDCF sensor, the pattern of the signals remains quite stable, indicating that the high-performance sensor enables to detect ultralow strains or deformations. Long-time stability and durability also play a vital role in the evolution of sensor performance. To further assess the stability of the sensor, a loading-unloading strain of 60% with a frequency of 0.5 Hz was applied to it for 6000 cycles. The electrical signals in Fig. 4e are stable throughout the whole process with minor fluctuation, illustrating the remarkable stability. The outstanding stability of the sensor is originated from the prominent robustness of Ecoflex,

corresponding mechanical output also remains steady during the process (Fig. S12). The strain-stress curve of the CDCF sensor in Fig. S13 shows that it has an appropriate flexibility, which is important to wearability. To evaluate the durability of the sensor over a long period time, we firstly applied a strain of 2% onto the sensor with the frequency of 0.5 Hz, then tested its electrical output after one week with the same parameters. The reproducible signals in Fig. S14 indicate that the sensor has a good durability.

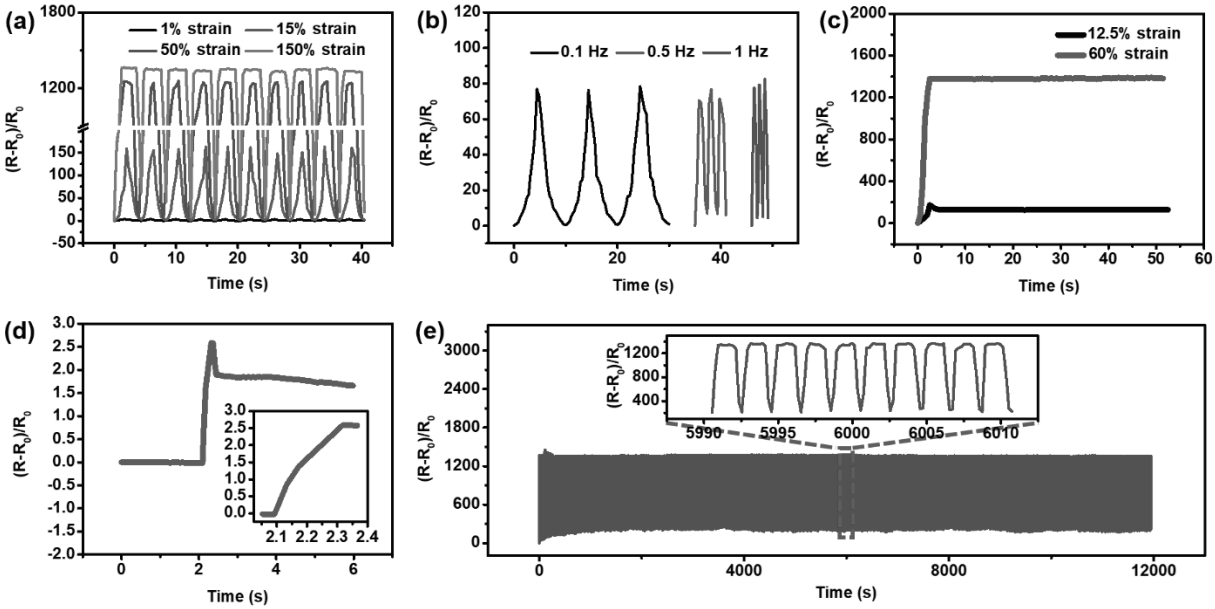

Fig. 4. Electromechanical property of the CDCF sensor. a) Electrical signals responding to various 10-cycle loading-unloading strain with the frequency of 0.25 Hz, and b) electrical response to stretching-releasing strain (10%) with different frequency, showing the dynamic stability in strain and frequency. c) The fractional change in resistance by applying step strains to the sensor to show its static reliability and low creep. d) The response speed (~225 ms) of the sensor reflected through applying a strain of 0.5% with the speed of 16 mm/s. e) The fractional change in resistance under the repeatable stretching-releasing strain of 60% for 6000 cycles with the frequency of 0.5 Hz, presenting the outstanding stability of the sensor.

3.4. Motion monitoring and identification by the strain sensor

Owing to the high sensitivity, large stretchability, fast response, prominent stability, and durability (see the performance comparison between the CDCF sensor and reported sensors in Table S2), the CDCF sensor can be employed to monitor many human body motions in real time. We firstly mount the high-performance sensor on the skin surface of the throat with viscous tape (Fig. S15a) to verify the availability in perceiving coughing, speaking, as well as water drinking. Fig. 5a displays the fractional change in resistance of the CDCF sensor during coughing. The signals climb and drop with the exertion and release of cough respectively, which is consistent with corresponding epidermis vibration. On the other hand, the response is repeatable throughout with marginal deviation, indicating the high reliability and stability in such motion detection. The sensor is also capable of sensing the epidermis and muscle vibration generated from speaking. Electrical output in Fig. 5b exhibits differentiable and reproducible patterns when speaking different words, showing great potential in the applications of phonation rehabilitation training as well as human-computer interaction. The electrical patterns from water drinking in Fig. 5c are reproducible, revealing the application foreground in the swallowing practice and training. Besides, by assembling the sensor on the skin surface of the wrist (Fig. S15b), various degrees of wrist bending can be recorded. Resistance signals generated from wrist bending with tiny and larger deformation in which the intensity rises and drops as a function of the degree of bending (Fig. 5d), showing the potential of wrist bending related movements such as the training of basketball shooting through suitably embedding the sensor in wristbands.

As a proof-concept demonstration of the sensor in the applications of monitoring and distinguishing motions, we develop an end-to-end healthcare system with the functions of respiration monitoring and recognition by combing the CDCF sensor with a convolutional neural network (CNN) model. The respiration signals are collected by attaching the CDCF sensor to the chest (Fig. S15c), then the respiration patterns (i.e. normal breath, tachypnea, and tachypnea with cough) are classified into three target classes by using the CNN (Fig. 5e). Fig. S16 and Fig. 5f show cyclic and typical patterns of respiration signals respectively, it can be observed that three signals have similar amplitude but distinguishable spectrums. Hence, we use the signal spectrum as the input of CNN for the classification. For the data preparation, the output of the CDCF sensor is filtered digitally using a sixth-order low-ass Butterworth filter with a 10Hz cut-off frequency, and is segmented using a 3s sliding window with 0.2s increment. The segmented data is then transformed by applying the fast Fourier transform (FFT), and splited into 80% and 20% for training and test set of CNN, respectively. The CNN architecture adopted in this work is shown in Fig. S17, which is composed of two convolutional layers i.e., a fully connected layer and a softmax classifier. The network is trained in a 32-sized mini-batch for 20 epochs using adaptive moment estimation (ADAM). The dynamic learning rate is 0.0001 with a decay rate of 0.001 for each iteration and the dropout rate is set to be 0.2. The confusion matrix for the test set in Fig. 5g shows that the classification accuracy can reach 93.3%. By taking advantage of the high-precision respiratory monitoring and recognition system, the sensor can be applied as an emergency alarm system for the healthcare of covid-19 infected patients, which is of significance to relieve the stress on medical care personnel.

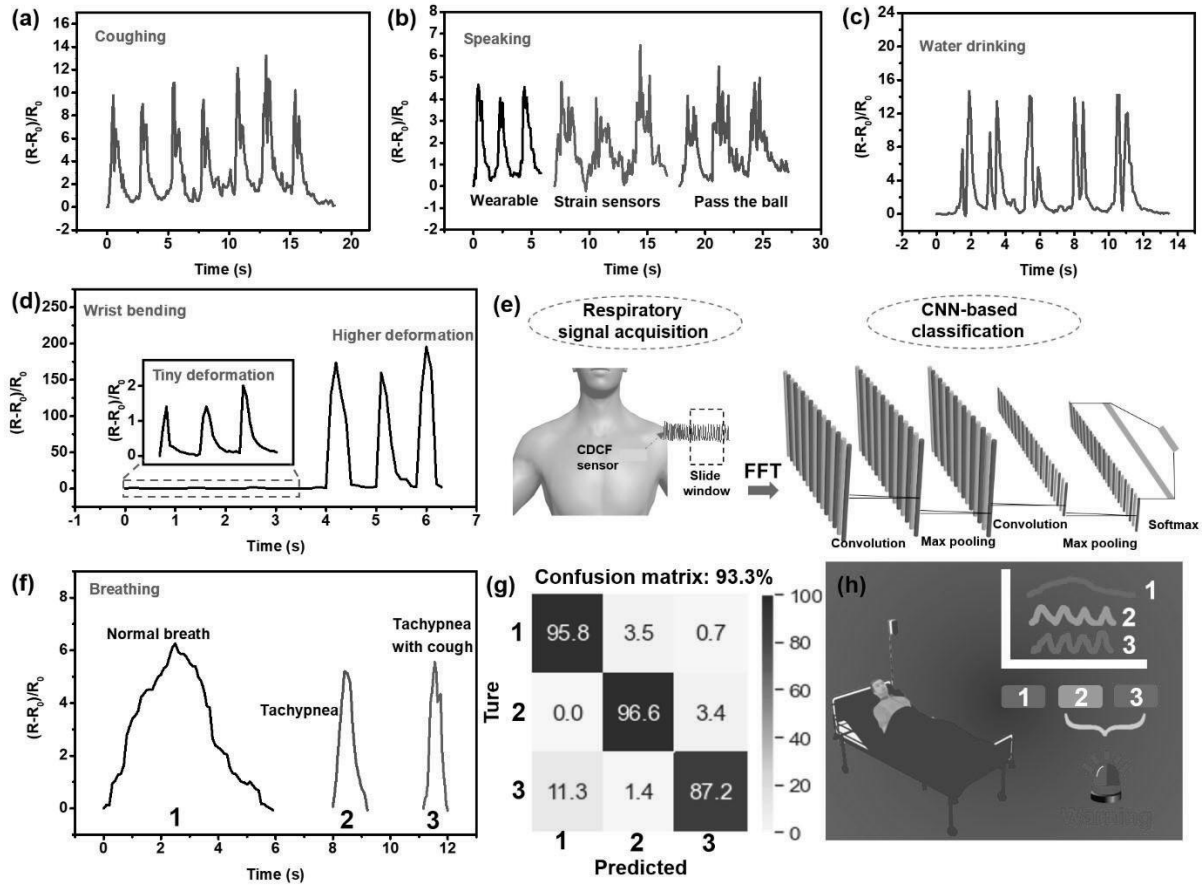

Fig. 5. The applications of the CDCF sensor in motion detection and identification. a) Ream-time detection of coughing, b) speaking, and c) water drinking by attaching the sensor to the throat. d) Detection of the wrist bending with tiny and larger deformation through mounting the sensor on the wrist. e) The schematic diagram of respiration monitoring and identification through integrating the CDCF sensor with a CNN model. f) Typical electrical outputs of normal breath, tachypnea, and tachypnea with cough respectively. g) Confusion matrix for the test set of the respiration monitoring and identification system, showing its high accuracy. h) Illustration showing the personal respiration monitoring and emergency warning system.

4. Conclusions

In summary, we have developed a high-performance stretchable strain sensor through carbonization and polymer-assisted copper deposition, based on cost-effective linen fabric. The assembling of copper on the fabric can significantly enhance both sensitivity (GF~3557.6 in the strain range from 0 to 48%, GF~47.8 in the strain range from 48% to 150%) and stretchability up to the strain of 300%, which is superior to the sensor made with CF (Stretchability up to the strain of 96% with the GF~23.0). The CDCF sensor with remarkable reliability and durability (>6000 cycles) can be dependably employed to perceive many motions in real time such as coughing, speaking, and wrist bending, etc. The healthcare system based on the sensor and a deep learning network shows the ability to monitor and distinguish normal breath, tachypnea, tachypnea along with cough with high accuracy, which is of great potential in the healthcare of patients with respiratory diseases. Particularly, the concept of assembling highly conductive elements on a conductive substrate to increase sensitivity and stretchability should be extended to many other strain sensors to improve their performance.

Conflicts of interest

The authors declare that they have no known competing financial interests or personal relationships that could have appeared to influence the work reported in this paper.

Acknowledgments

We would like to thank the funding supports by EU Horizon 2020 through project ETEXWELD-H2020-MSCA-RISE-2014 (Grant No. 644268), the University of Manchester

through UMRI project “Graphene-Smart Textiles E-Healthcare Network” (AA14512), as well as Key Laboratory of Silk Culture Heritage and Products Design Digital Technology, Ministry of Culture and Tourism, P. R. China (2020WLB02).

References

[1] S. Wang, Y. Fang, H. He, L. Zhang, C.a. Li, J. Ouyang, Wearable Stretchable Dry and Self- Adhesive Strain Sensors with Conformal Contact to Skin for High- Quality Motion Monitoring, Adv. Funct. Mater. 31 (2021) 2007495.

[2] H. Zhou, Z. Wang, W. Zhao, X. Tong, X. Jin, X. Zhang, Y. Yu, H. Liu, Y. Ma, S. Li, Robust and sensitive pressure/strain sensors from solution processable composite hydrogels enhanced by hollow-structured conducting polymers, Chem. Eng. J. 403 (2021) 126307.

[3] Z. Liu, Y. Zheng, L. Jin, K. Chen, H. Zhai, Q. Huang, Z. Chen, Y. Yi, M. Umar, L. Xu, Highly Breathable and Stretchable Strain Sensors with Insensitive Response to Pressure and Bending, Adv. Funct. Mater. (2021) 2007622.

[4] M. Wang, Z. Yan, T. Wang, P. Cai, S. Gao, Y. Zeng, C. Wan, H. Wang, L. Pan, J. Yu, Gesture recognition using a bioinspired learning architecture that integrates visual data with somatosensory data from stretchable sensors, Nat. Electron. 3 (2020) 563-570.

[5] O.A. Araromi, M.A. Graule, K.L. Dorsey, S. Castellanos, J.R. Foster, W.-H. Hsu, A.E. Passy, J.J. Vlassak, J.C. Weaver, C.J. Walsh, Ultra-sensitive and resilient compliant strain gauges for soft machines, Nature. 587 (2020) 219-224.

[6] L. Xu, Z. Liu, H. Zhai, X. Chen, R. Sun, S. Lyu, Y. Fan, Y. Yi, Z. Chen, L. Jin, J. Zhang, Y. Li, T.T. Ye, Moisture-Resilient Graphene-Dyed Wool Fabric for Strain Sensing, ACS Appl. Mater. Interfaces. 12 (2020) 13265-13274.

[7] S. Seyedin, S. Uzun, A. Levitt, B. Anasori, G. Dion, Y. Gogotsi, J.M. Razal, MXene composite and coaxial fibers with high stretchability and conductivity for wearable strain sensing textiles, Adv. Funct. Mater. 30 (2020) 1910504.

[8] Z. Tang, S. Jia, F. Wang, C. Bian, Y. Chen, Y. Wang, B. Li, Highly stretchable core–sheath fibers via wet-spinning for wearable strain sensors, ACS Appl. Mater. Interfaces. 10 (2018) 6624-6635.

[9] F. Liu, Y. Dong, R. Shi, E. Wang, Q. Ni, Y. Fu, Continuous graphene fibers prepared by liquid crystal spinning as strain sensors for Monitoring Vital Signs, Mater. Today Commun. 24 (2020) 100909.

[10] Y. Yang, L. Shi, Z. Cao, R. Wang, J. Sun, Strain sensors with a high sensitivity and a wide sensing range based on a Ti3C2Tx (MXene) nanoparticle–nanosheet hybrid network, Adv. Funct. Mater. 29 (2019) 1807882.

[11] C. Wang, X. Li, E. Gao, M. Jian, K. Xia, Q. Wang, Z. Xu, T. Ren, Y. Zhang, Carbonized Silk Fabric for Ultrastretchable, Highly Sensitive, and Wearable Strain Sensors, Adv. Mater. 28 (2016) 6640-6648.

[12] M. Zhang, C. Wang, H. Wang, M. Jian, X. Hao, Y. Zhang, Carbonized cotton fabric for high- performance wearable strain sensors, Adv. Funct. Mater. 27 (2017) 1604795.

[13] C. Wang, M. Zhang, K. Xia, X. Gong, H. Wang, Z. Yin, B. Guan, Y. Zhang, Intrinsically stretchable and conductive textile by a scalable process for elastic wearable electronics, ACS Appl. Mater. Interfaces. 9 (2017) 13331-13338.

[14] W. Qi, M. Jian, C. Wang, Y. Zhang, Carbonized Silk Nanofiber Membrane for Transparent and Sensitive Electronic Skin, Adv. Funct. Mater. 27 (2017) 1605657.

[15] C. Wang, K. Xia, M. Jian, H. Wang, M. Zhang, Y. Zhang, Carbonized silk georgette as an ultrasensitive wearable strain sensor for full-range human activity monitoring, J. Mater. Chem. C. 5 (2017) 7604-7611.

[16] Z. Liu, K. Chen, A. Fernando, Y. Gao, G. Li, L. Jin, H. Zhai, Y. Yi, L. Xu, Y. Zheng, Permeable graphited hemp fabrics-based, wearing-comfortable pressure sensors for monitoring human activities, Chem. Eng. J. 403 (2021) 126191.

[17] K. Xia, X. Chen, X. Shen, S. Li, Z. Yin, M. Zhang, X. Liang, Y. Zhang, Carbonized Chinese art paper-based high-performance wearable strain sensor for human activity monitoring, ACS Appl. Mater. Interfaces. 1 (2019) 2415-2421.

[18] S.Y. Cho, Y.S. Yun, S. Lee, D. Jang, K.-Y. Park, J.K. Kim, B.H. Kim, K. Kang, D.L. Kaplan, H.-J. Jin, Carbonization of a stable β-sheet-rich silk protein into a pseudographitic pyroprotein, Nat. Commun. 6 (2015) 1-7.

[19] P. Li, Y. Zhang, Z. Zheng, Polymer- Assisted Metal Deposition (PAMD) for Flexible and Wearable Electronics: Principle, Materials, Printing, and Devices, Adv. Mater. 31 (2019) 1902987.

[20] J. Chang, J. Shang, Y. Sun, L.K. Ono, D. Wang, Z. Ma, Q. Huang, D. Chen, G. Liu, Y. Cui, Flexible and stable high-energy lithium-sulfur full batteries with only 100% oversized lithium, Nat. Commun. 9 (2018) 4480.

[21] T. Yamada, Y. Hayamizu, Y. Yamamoto, Y. Yomogida, A. Izadi-Najafabadi, D.N. Futaba, K. Hata, A stretchable carbon nanotube strain sensor for human-motion detection, Nat. Nanotechnol. 6 (2011) 296.

[22] K.-H. Kim, S.K. Hong, S.-H. Ha, L. Li, H.W. Lee, J.-M. Kim, Enhancement of linearity range of stretchable ultrasensitive metal crack strain sensor via superaligned carbon nanotube-based strain engineering, Mater. Horiz. 7 (2020) 2662-2672.